Reprinted from Preprint Volume: 17th Conference on Radar Meteorology, Oct. 26-29, 1976; Seattle Wash.; Published by American Meteorological Soc., Boston, Ma.

WIND AND DIVERGENCE MEASUREMENTS IN EXTRATROPICAL CYCLONES FROM DOPPLER RADAR

Harold W. Baynton, Charles L. Frush, and Robert J. Serafin

National Center for Atmospheric Research[1]
Boulder, Colorado

Peter V. Hobbs, Robert A. Houze, Jr., and John D. Locatelli

Department of Atmospheric Sciences
University of Washington
Seattle, Washington

1. INTRODUCTION

An NCAR C-band Doppler radar has been used to obtain measurements in extratropical cyclonic storms in the Pacific Northwest for two winters as part of the University of Washington's CYCLES (Cyclonic Extratropical Storms) PROJECT. The radar is equipped with a real-time Doppler processor (Lhermitte, 1972) and a color display (Gray *et al.*, 1975) for showing velocities or range-normalized reflectivities. As the antenna was rotated about a vertical axis at a series of constant elevation angles, detailed velocity-azimuth displays (VAD) were obtained of the radial component of the target velocity. Each display was portrayed in fifteen colors with a resolution of 2 m s $^{-1}$.

This paper describes how the color display provides qualitative and quantitative information on the wind field during VAD scans. Techniques of pattern recognition are described for detecting veering and backing winds and jets. Confluence and difluence are also detectable and the presence of convergence is sometimes evident from inspection of the display. Procedures for computing wind profiles and convergence are given and the results of such computations are presented.

2. THE ELEMENTS OF COLORED DOPPLER VELOCITY PATTERNS

Pulsed Doppler radars are characterized by a maximum unambiguous velocity (V_{max}) given by

$$V_{max} = (PRF)\frac{\lambda}{4} \qquad (1)$$

where PRF is the pulse repetition frequency in hertz, and λ is the radar wavelength in meters. For the NCAR C-band radar, λ = 0.0545 m, and for the CYCLES PROJECT the PRF was set at 1071 Hz. Hence V_{max} = 14.60 m s $^{-1}$.

Velocities greater than the maximum unambiguous velocity are "folded over" and then assigned velocities less than the maximum unambiguous velocity. In practice with the color display there is no difficulty in resolving these ambiguities, provided that the targets are continuous. Velocities ranging between $\pm |V_{max}|$ are assigned, unambiguously, one of fifteen colors. In the CYCLES PROJECT, the width of each color band was thus simply 2(14.60)/15=1.95 m s $^{-1}$. Grey is used to indicate targets with radial velocities of 0 ±0.97 m s $^{-1}$. Ground clutter, as well as all targets viewed from the side, no matter how fast they are moving, have zero radial velocity and therefore appear grey.

The TV monitor or color display can be thought of as a fine mesh grid. Each square of the grid is assigned one of the fifteen colors corresponding to the observed radial velocity of targets, or black if there are no targets. The fifteen colors are also numbered sequentially, +7 through 0 to -7, where +7 and -7 correspond to the maximum unambiguous velocity away from and toward the radar. If the velocity toward the radar rises above 14.60 m s $^{-1}$ (in magnitude), the display will shift from color -7 (purple) to +7 (red). If further increases occur, the colors will sequence through +6, +5, etc. The 15th color in this kind of sequence is grey, which would represent 29.2±0.97 m s $^{-1}$ in magnitude, the sign being determined by the context. Clearly, if the target is a continuous one extending all the way out from the radar there is no ambiguity. However, with isolated targets there is ambiguity since the same color might have several meanings.

Also contributing to the patterns on the TV monitor is the increase in height of the radar beam with increasing slant range. Using the 4/3-earth-radius convention (Battan, 1973, p.24) to allow for average refraction and earth curvature, we have

$$Z = \frac{R^2}{17{,}000} + R \sin \alpha \qquad (2)$$

where Z is the height (in km) of the beam above the radar at slant range R (in km) and α is the elevation angle. Finally, since strong thermal gradients characterize extratropical cyclones, winds change in both direction and speed with changing height.

To illustrate how these elements are combined by the color display into a colored picture, we consider the mean winter wind profile for Seattle.

[1] The National Center for Atmospheric Research is sponsored by the National Science Foundation.

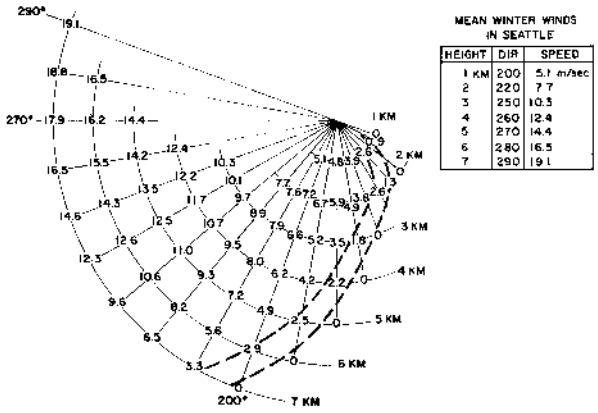

Fig. 1 Radial components of mean winter winds at Seattle. Coordinates are azimuth (in °) and slant range corresponding to beam heights of 1-7 km. Dashed lines show boundaries of the dark green region on the radar color display.

Fig. 1 shows the distribution of radial components, with slant range and azimuth, for this average profile. Concentric arcs on the figure are drawn at increasing slant ranges to correspond to beam heights of 1, 2, 3, 4, 5, 6, and 7 km. Radial components are then plotted along each height contour. The dashed lines show where the boundaries of the dark green color (number -1) would lie. When Fig. 1 is expanded to the full circle and radial velocity contours are drawn at the color boundaries, Fig. 2 is obtained. Observing that winds veer with height for this profile, we note that the zero-velocity band (grey on the color display) bisects the picture in the shape of an S. When winds back with height, the grey band traces a backwards S.

3. PATTERN RECOGNITION

Qualitative information, concerning bulk pro properties of the air flow, is available in real-time based on pattern recognition. Some examples are given below.

3.1 Patterns Typical of Warm Air Advection and Warm Fronts

When there is warm air advection, winds veer with height and, as we have already seen from our consideration of the mean winter wind profile, the band of zero velocities then bisects the display in the shape of an S. Color displays with this feature were common in the CYCLES PROJECT during the winters of 1974-75 and 1975-76. Fig. 3, observed at 2205 PST on 13 January 1976, is typical. Fig. 3 also illustrates a feature of the color display whereby any of the fifteen colors -- here grey -- can be replaced by white.

When the radar beam penetrates a warm front, an S-shaped warm advection pattern is seen on the color display in the baroclinic zone below the frontal surface, with little evidence of wind shear appearing in the relatively uniform air mass above the warm frontal surface. An example of a warm frontal pattern was observed at 2036 PST on

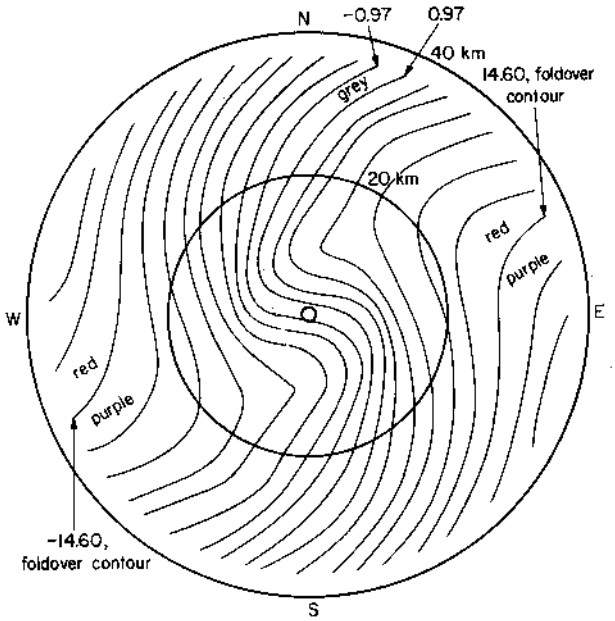

Fig. 2 Contours of radial components constructed from the mean winter wind profile for Seattle for an elevation angle of 11°. Contours are drawn at intervals of 1.95 m s^{-1} corresponding to the width of each color band in the color display.

26 January 1976 (Fig. 4). With the echo extending to a height of 5 km, virtually all of the wind shear occurred below 1.2 km, the apparent height of the warm frontal surface.

3.2 Patterns Typical of Occlusions

Complex thermal gradients are typically associated with occlusions (e.g. see Kreitzberg, 1964; Elliott and Hovind, 1965; Kreitzberg and Brown, 1970; Browning et al., 1973; Houze et al., 1976). Cold advection in the lowest layers might be accompanied by warm advection aloft or vice versa. During January 1976 mixed patterns of two types were observed. A striking example of warm advection below and cold advection aloft was observed on 22 January. Fig. 5 is the color display obtained at 0705 PST. The picture was bisected by a perfect S between the surface and 1.9 km, above 1.9 km the pattern was reversed by backing winds. Fig. 6 is a black and white drawing based on Fig. 5 showing a wind profile derived from the colored velocity pattern. The procedure for obtaining the wind profile is explained in the caption of Fig. 6. Hodographs for the layers 0.4 to 1.9 km and 1.9 to 4.2 km, included as inserts in Fig. 6, verify the presence of warm advection in the lower layer and cold advection in the upper layer.

3.4 The Identification of Jets

Jets are frequently observed as concentric color rings around a maximum core. One may be seen inside the inner range mark in Fig. 3. The storm of 14 January 1976, producing the display shown in Fig. 7, featured two jets, one at about 1.8 km and another at about 4 km. These jets are layers of maximum wind speed. Although the color display provides no information as to the lateral extent of a jet, it gives estimates of height and

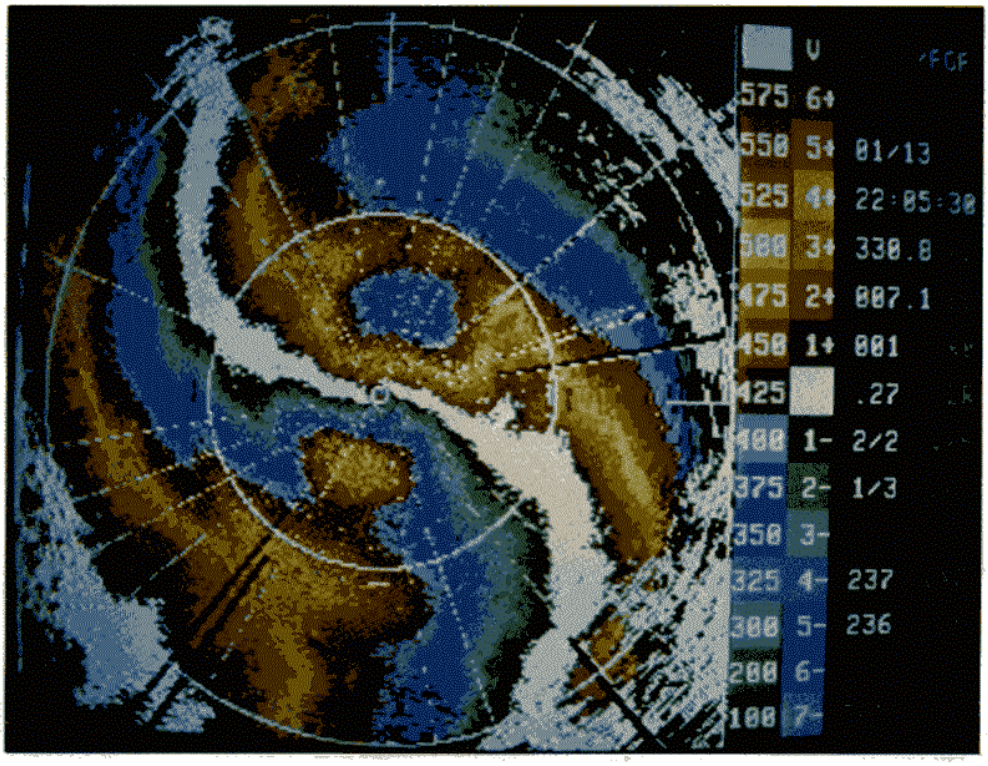

Fig. 3 Color display typical of warm air advection without a front. Picture is for 2205 PST, 13 January 1976, Tacoma, elevation 7.1°. Range marks at 20 and 40 km, N at top of picture, velocity color code in the right column. The zero-velocity band bisecting the picture in the shape of an S indicates winds veering from South near the ground to WSW aloft. Continuing color changes to the WSW and ESE out to full range also indicate that thermal gradients extend to the echo top.

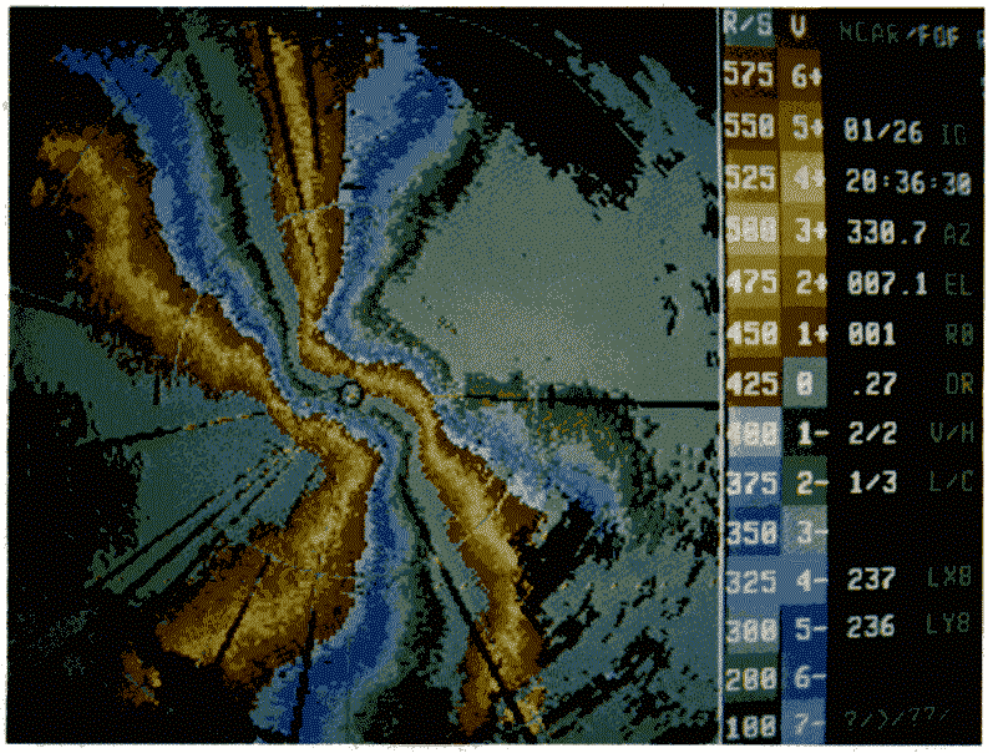

Fig. 4 Color display typical of a warm front. Picture is for 2036 PST, 26 January 1976, Tacoma, elevation 7.1°, range marks at 20 and 40 km. Confinement of the S-shape of the zero-velocity band to the lowest 1.2 km (to 10 km slant range), and the two pie-shaped grey wedges extending in from 40 to 10 km slant range, indicate that the thermal gradient is confined to the lowest 1.2 km and place the warm frontal surface at 1.2 km.

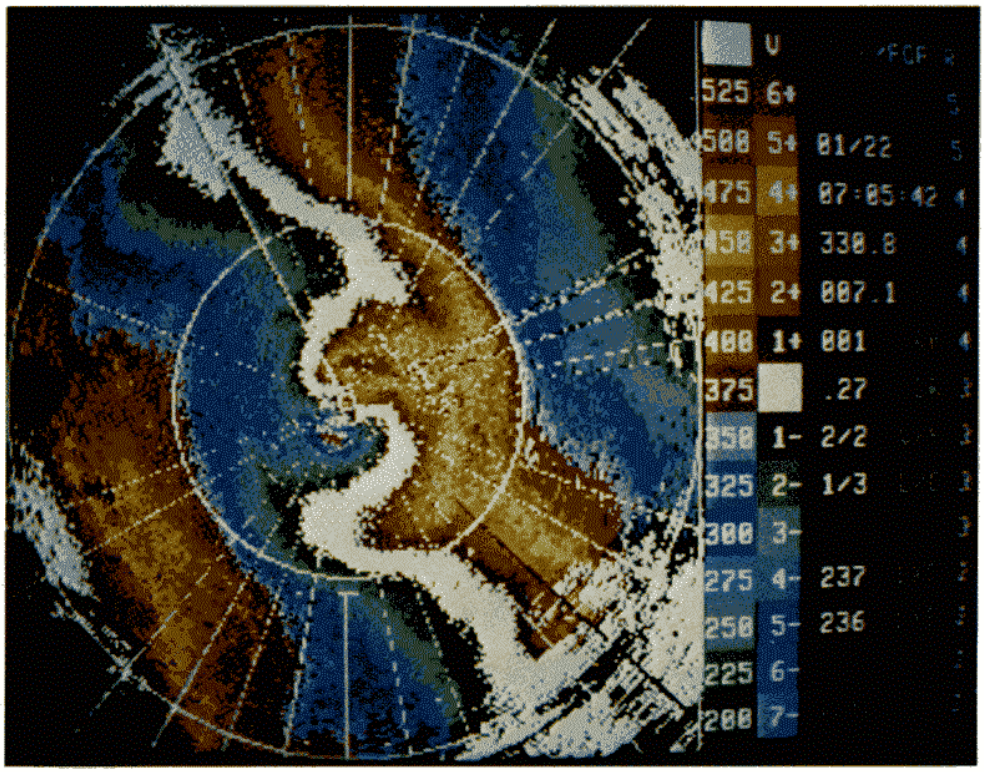

Fig. 5 Color display typical of an occulsion with warm air advection near the surface and cold air advection aloft. Picture is for 0705 PST, 22 January 1976, Tacoma, elevation 7.1°, range marks at 20 and 40 km. The S within 15 km slant range indicates veering winds and warm air advection to a height of 1.9 km. Beyond 15 km the zero-velocity band traces a counter-clockwise spiral, indicating backing winds and cold air advection.

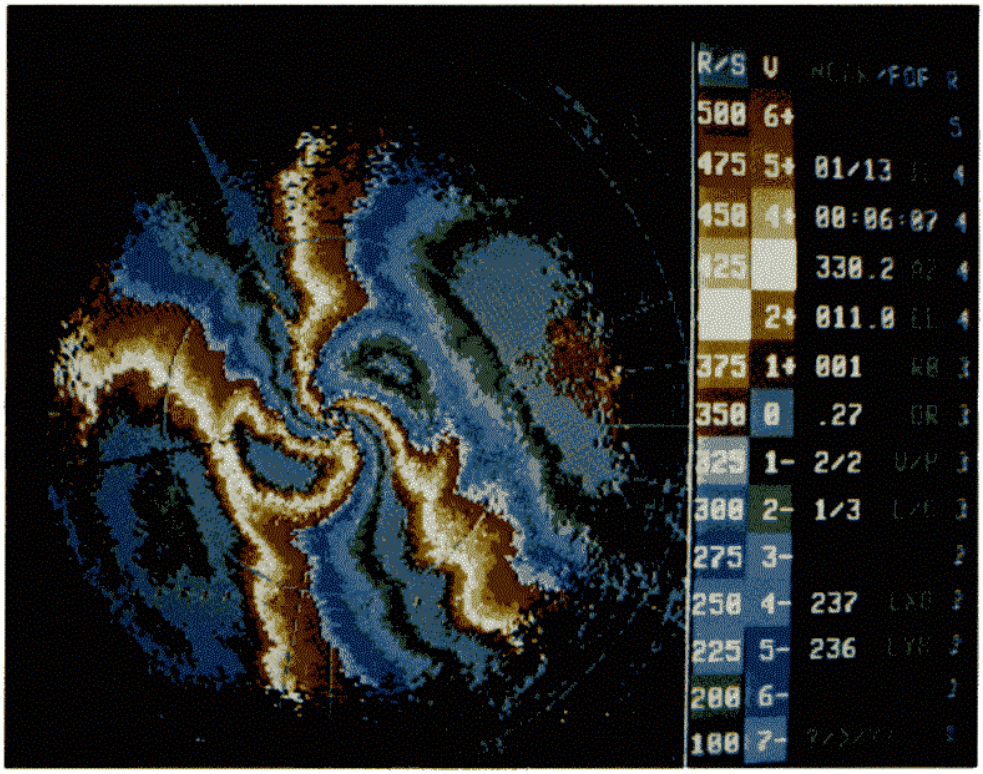

Fig. 7 Color display of two jets at 0006 PST, 14 January 1976 (date incorrect in picture). Elevation 11°, range marks at 20 and 40 km. Jets produce a pair of oval-shaped rings, upwind and downwind. The lower jet is horizontal, appearing at the same slant range (10 km) both upwind and downwind. The upper jet slopes upward, appearing at a greater slant range upwind than downwind.

magnitude both upwind and downwind. Height is determined from the slant range and elevation using Eq. (2). The range marks are at 20 and 40 km.

From the upwind and downwind estimates of height many of the jets are seen to slope upwards. On 14 January 1976 the upper jet has an upward slope of 1:30 or 1.8°. The lower jet is nearly horizontal. Although several upward sloping jets, typically about 1:90 or 0.6°, have been noted, no downward sloping jets have been observed. The radar dish is aligned to an accuracy of 0.1° using a plumb bob, a clinometer, and the sun's C-band radiations as a target with known coordinates. Consequently observed slopes of 0.6 to 1.8° must be accepted as real.

It is tempting to assume that the air is itself sloping upwards within the jet since this would provide a direct estimate of vertical velocities in the system. Such an interpretation on the upper jet of Fig. 7 would imply an upward velocity of 1 m s $^{-1}$. However, it has not yet been possible to compare vertical velocities implied by a sloping jet to other independent measurements.

3.5 Asymmetric Patterns

If the wind field within the echo region is uniform, the echo will exhibit symmetry. At any slant range the maximum radial components towards and away from the radar will be equal and the two direction estimates, obtained from the azimuths of the zero-velocity band on opposite sides of the radar, will be equal. Asymmetric patterns can be related to some non-uniformity of the wind field. The example of an upward sloping jet has already been given. The evidence was that the slant range of the jet was greater downwind than upwind Another kind of asymmetry is evident in Fig. 4, which shows a display typical of a warm front. It is also a good example of difluence.

A quick test for difluence or confluence is to lay a straight edge across the display from the middle of the zero-velocity band on one side and through the center of the display. If the straight edge does not intercept the middle of the band at the same range on the opposite side of the radar, the flow is either difluent or confluent. Applying this test to Fig. 4, at a slant range of 40 km (Z = 5 km), shows that the wind direction is 247° north of the radar and 260° south of the radar.

Occasionally convergence may be suspected by inspection of the color display. Fig. 3 is an example. At a slant range of 20 km (Z = 2.5 km) the maximum radial speed downwind (northeast sector) nearly coincides with the "folded over" contour (red to purple) of 14.60 m s $^{-1}$, whereas, upwind of the radar (southwest sector) the display shows three colors, or nearly 6 m s $^{-1}$ greater than the "folded over" contour. The discussion in § 5 verifies the presence of convergence, at the same height, 30 min. later than the time of Fig. 3.

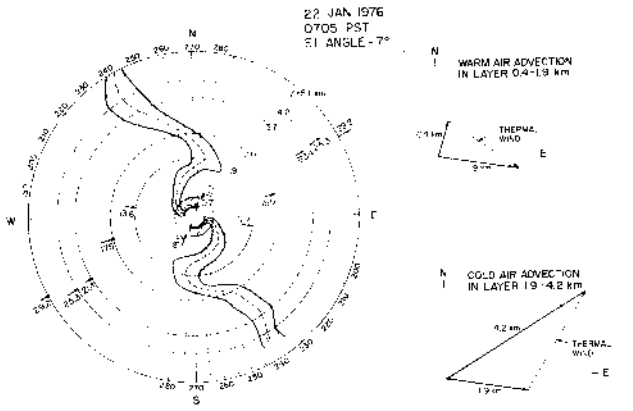

Fig. 6 Elements derived from the color display shown in Fig. 5. Wind directions are obtained from the zero-velocity band bisecting the figure by subtracting 90° from the azimuth on the low pressure (NW) side or adding 90° to the azimuth on the high pressure (SE) side. The two direction scales make this adjustment. Upwind and downwind speeds read from the color display are shown on the height contours. The hodographs confirm warm air advection in the layer of veering winds and cold air advection in the layer of backing winds.

4. COMPARISON WITH RAWINSONDE DATA

Wind profiles were obtained from the radar color display using the procedure described in the caption of Fig. 6. Three comparisons between radar wind profiles and simultaneous rawinsonde data, obtained at the University of Washington in Seattle, 45 km north of the radar site, are illustrated in Fig. 8. Since the observations were taken during periods of frontal passages, some differences in the soundings, due to atmospheric spatial variations, are to be expected. In spite of this, the results from the two independent methods are very similar.

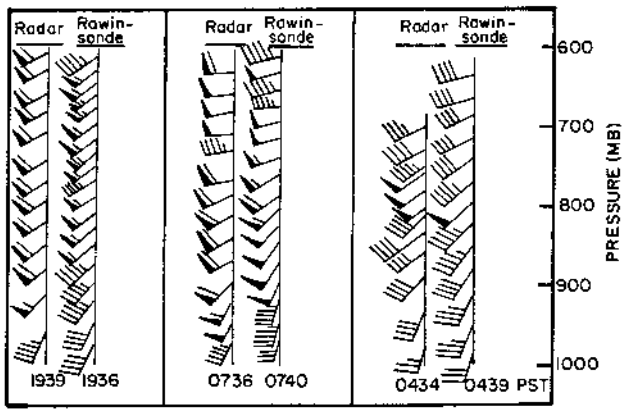

Fig. 8 Comparison of radar and rawinsonde wind data for 10 January 1976. Half wind barb is for 2.5 m s^{-1}, full barb is for 5 m s^{-1}, and flag is for 25 m s^{-1}.

During periods of precipitation, radar-derived winds can be obtained at intervals as close together as 7 min., thus providing a valuable supplement to conventional rawinsonde data, which can usually be obtained no more frequently than every 45 min.

5. DIVERGENCE ESTIMATES

Procedures for estimating divergence and convergence from Doppler radar data are described by Caton (1963) and by Browning and Wexler (1968). While their techniques were applied to tape recorded data, the underlying principles are readily adapted to photographs of the color display.

Divergence may be evaluated from the expression:

$$\text{Divergence} = \frac{2}{R}\left(\frac{\bar{V}}{\cos\alpha} - \bar{V}_f \tan\alpha\right) \qquad (3)$$

where V is the average radial velocity at an elevation angle α and a slant range of R during a 360° scan, and $\bar{V}_f$ is the fall speed of the precipitation particles. R is expressed in meters; velocities are in m s $^{-1}$, positive away from the radar.

Generally one is interested in a vertical profile of divergence, and in order that the profile may apply over the same horizontal area one must use a series of scans at different elevation angles. Our procedure is to compute $\bar{V}$ at a slant range of 20 km, the inner range marker on the color display, at elevation angles of 4, 7, 11, 15, and 19° corresponding to heights of 1.55, 2.59, 3.97, 5.33, and 6.66 km above mean sea level. This series of scans is completed in about 4 min. The choice of 20 km complies with Browning and Wexler's recommendation that the slant range should be $\geq$ 23 km in order to reduce height errors.

Color transparencies for each elevation angle are projected onto polar coordinate graph paper. The 20-km range mark and the location of all color transitions at 20 km are traced in pencil onto the graph paper. The angle subtended by each color band (of known speed) at a range of 20 km is read directly on the graph paper and the mean wind for a full 360° scan is readily computed.

Vertical velocities of precipitation particles [V_f in Eq. (3)] can be estimated by pointing the antenna vertically. During the CYCLES PROJECT vertically pointing scans were interspersed regularly with the VAD scans. Generally small fall speeds, characteristic of snow, were observed as one would expect with the low freezing levels. Fall speed spectra were recorded during the CYCLES PROJECT and these spectra have been used to remove the influence of ground clutter in estimating average vertical velocities of the precipitation particles. During 23 min. of vertical scanning, between 2208 and 2258 PST on the 13 January 1976, the vertical velocities given in Table 1 were observed.

These values of $\bar{V}_f$ are believed to be representative of Pacific Northwest storms and apply specifically to the divergence profile at 2237 PST on 13 January 1976 that appears in line 1 of Table 2.

The estimates of $\bar{V}$ obtained as described above and the values of $\bar{V}_f$ in Table 1 are substituted in Eq. (3) to obtain the profiles given in Table 2.

The three divergence profiles in Table 2 relate to Figs. 3, 4, and 5. The magnitudes of the computed divergences are consistent with the results of Matsumoto *et al.* (1967) who found, from measurements with closely spaced rawinsondes, that divergences in the mesoscale precipitation areas of winter storms over Japan were $\approx 10^{-4}$ s^{-1}.

Table 1. Mean vertical velocities of precipitation particles, ground clutter effects removed, between 2208 and 2258 PST, 13 January 1976. (Velocities positive upward).

Height (km, above MSL)	1.55	2.59	3.97	5.33	6.66
$\bar{V}_f$ *(m s^{-1})*	-1.9	-1.2	-1.0	-0.8	-0.7

Table 2. Profiles of divergence observed at Tacoma. Units are 10^{-4} s^{-1}. (Negative sign indicates convergence.)

		Height (km above MSL)				
Time (PST)	*Date*	*1.55*	*2.59*	*3.97*	*5.33*	*6.66*
2237	13 Jan.	-1.60	-1.11	-0.51	+0.93	+1.39
0705	22 Jan.	-0.06	-0.97	+0.90	+0.12	+0.87 at Z=6.17 km
2036	26 Jan.	0.29	0.15	0.46	0.64	no echo

In Table 2, the 13 January case shows low level convergence and high level divergence. The 22 January profile is a confused mixture, perhaps not unexpected in view of the confused wind profile shown in Fig. 5. The 26 January case shows divergence at all levels. Difluence had been detected at 5 km in Fig. 4.

6. CONCLUSIONS

Experience using the NCAR CP-3 radar in the University of Washington's CYCLES PROJECT has shown that colored Doppler velocity patterns in VAD format provide a variety of useful information on the wind field in situations of widespread precipitation. This information includes wind speed and direction as a function of height and divergence which can be computed from pictures of the radar color display with suitable speed and accuracy for mesoscale studies.

In real time, readily recognizable patterns in the colored VAD displays have shown warm and cold advection layers, jets, and zones of difluence or confluence. Warm advection is indicated by an S-shaped zero velocity band, while cold advection is indicated by a backwards S. Jets (maximum wind layers) appear as concentric color rings around a maximum core. Difluence or confluence is indicated by an asymmetry in the zero-velocity band.

Acknowledgments: The CYCLES PROJECT is supported by Grant ATM 74-14726-A02 to the University of Washington from Atmospheric Sciences Section of the National Science Foundation. The successful operation of the radar was due to the skill and dedication of NCAR technicians Robert Bowie, Alan Sorenson, and Dale Zalewski. Richard Bobka assisted in assembling and dismantling the radar on site and Thomas J. Matejka and Dan Willott of the University of Washington assisted in the collection of data.

REFERENCES

Battan, L.J., 1973: *Radar observation of the atmosphere.* The University of Chicago Press, 324 pp.

Browning, K.A. and R. Wexler, 1968: The determination of kinematic properties of a wind field using Doppler Radar. *J. Appl. Met.*, 7, 105-113.

_____, M.E. Hardman, T.W. Harrold and C.W. Pardoe, 1973: The structure of rainbands within a mid-latitude depression. *Quart. J. Roy. Met. Soc.*, 99, 215-231.

Caton, P.A.F., 1963: Wind measurement by Doppler radar. *Meteor. Mag.*, 92, 213-222.

Elliott, R.D. and E.L. Hovind, 1965: Heat, water, and vorticity balance in frontal zones. *J. Appl. Met.*, 4, 196-211.

Gray, G.R., R.J. Serafin, D. Atlas, R.E. Rinehart, and J.J. Boyajian, 1975: Real-time color Doppler radar display. *Bull. Am. Met. Soc.*, 56, 580-588.

Houze, R.A., Jr., J.D. Locatelli and P.V. Hobbs, 1976: Dynamics and cloud microphysics of the rainbands in an occluded front. *J. Atmos. Sci.*, in press.

Kreitzberg, Carl W., 1964: The structure of occlusions as determined from serial ascents and vertically-directed radar. Res. Rep. AFCRL-64-26, Air Force Cambridge Research Laboratories, L.G. Hanscom Field, Mass. 121 pp.

_____, and H.A. Brown, 1970: Mesoscale weather systems within an occlusion. *J. Appl. Met.*, 9, 417-432.

Lhermitte, R.M., 1972: Real time processing of meteorological Doppler radar signals. *Preprints 15th Radar Meteorology Conf.*, Boston, Amer. Meteor. Soc., 364-367.

Matsumoto, S., K. Nimomiya, and T. Akiyama, 1967: Cumulus activities in relation to the mesoscale convergence field. *J. Met. Soc. Japan*, 45, 292-304.

CORRIGENDUM: See color pages of this article, Fig. 7. The last sentence of the caption should read, "The upper jet slopes upward, appearing at a greater slant range downwind than upwind."